Formation of anionic excitations in the rare-gas solids and their coupling to dissociative states of adsorbed molecules

P. Rowntree
Department of Nuclear Medicine and Radiobiology, Université de Sherbrooke, Sherbrooke, Québec, Canada J1H 5N4

H. Sambe
Department of Chemistry, George Washington University, Washington, D.C. 20052

L. Parenteau and L. Sanche
Department of Nuclear Medicine and Radiobiology, Université de Sherbrooke, Sherbrooke, Québec, Canada J1H 5N4
(Received 19 May 1992; revised manuscript received 26 October 1992)

It is experimentally demonstrated that (electron plus exciton) core-excited resonances are formed by low-energy electron scattering in the Ar, Kr, and Xe rare-gas solids at 11.6±0.2, 9.7±0.2, and 7.7±0.2 eV, respectively. These resonance states can be efficiently coupled with dissociative Rydberg anion states of adsorbed H_2O, C_2D_6, and C_6D_6, but not with valence-dissociative states of adsorbed O_2 or C_6D_6. These resonances are revealed as narrow (full width at half maximum $\Delta E = 0.2-0.4$ eV) enhancements in the dissociative attachment yields of the adsorbed molecular species, at incident electron energies just below that of exciton formation in the condensed rare gases. Above the exciton energies, in contrast, the dissociative attachment mechanism in the adsorbed molecules can be attenuated, or completely quenched. All observations are characterized as "quasi-two-electron-jump" processes due to sizable overlaps between the associated Rydberg orbitals.

I. INTRODUCTION

In recent years the interaction between electronically excited solids and adsorbed (or solvated) molecular species has been shown to facilitate important photochemical mechanisms and has been demonstrated to have significant potential for the selective modification of solids and adsorbate systems. These processes include, but are not limited to, the oxidation of semiconductor surfaces,[1-3] molecular fragmentation via photoelectron attachment,[4-6] charge separation of di-halogen species,[7,8] and the efficient preparation of excited species via excitation transfer from the host solid to the dopant species.[9] Following the results of Marsh *et al.*,[5] several groups have found that excitations of metal substrates induced by the absorption of UV radiation can cause the desorption and dissociation of many molecular adsorbates; the mechanisms for this coupling include direct excitation of the (adsorbate+substrate) system, and the attachment of photogenerated electrons to the adsorbate, leading to dissociative electron attachment (DEA). These photoelectron driven processes can occur for electrons excited to above or just below the vacuum level of the substrate. Investigations of the nature of the initially excited states of the solid "host," and the nature of the coupling with the target species, have increased our understanding of energy deposition, transport, and trapping (localization) processes in the solid phase, especially for metal and semiconductor surfaces.

In addition to the work on metal and semiconductor surfaces, there is a growing body of results obtained using optical excitation of molecular solids, leading to exciton formation; the temporal and spatial evolution of the excited states can be used to determine exciton diffusion parameters, trapping probabilities, and excitation transfer probabilities. The rare-gas solids (RGS) of Ne, Ar, Kr, and Xe have been instrumental in these works because they provide an almost perfectly inert host matrix and because the exciton energies of the RGS (8–16 eV) are similar to or greater than the energies of the first excited states of most molecular species. In the simplest conception of this class of experiments, the target species of interest is dissolved in a rare-gas matrix or on a multilayer film. The host+target matrix system is then photolyzed at wavelengths corresponding to the excitation of the RGS, and the consequences of excitation transfer are measured, such as photoelectron yields from the target species,[10,11] molecular luminescence,[12] or molecular dissociation.[7,8] By considering the sensitivity of the transfer process to the thickness and composition of the host+target matrix, it is possible to determine the mobility of the initially prepared excitonic states of the solid, as well as characterize the various quenching processes which reduce the effective transfer probabilities of the initial excitation to the target species.

Even though many different types of particles could be utilized to initially excite molecular solids and rare-gas matrices, the experimental emphasis to date has been on initial excitations which can be prepared optically. However, much of the work cited above could be performed using low-energy electrons as a source of the initial excitation. Electron stimulated desorption (ESD) measurements of atoms and molecules in their ground or metastable states are illustrative of the excitation transfer processes which have been measured using low-energy electrons as the primary energy source.[13] Of course, there

are basic differences between the interactions of electrons and photons in the molecular solid which may have determinant implications for the energy deposition, and the subsequent transport, exchange, and localization processes in solids and at their surfaces. The formation of transient intermediate anions (combining an energetic incident electron with one of the atoms or molecules of the solid) is probably the most important consequence of these differences in the mechanism of the primary interaction.[14] Such transient anion states can either decay by ejecting the additional electron, by capturing it permanently, or by dissociating into a stable anion fragment and a neutral fragment. This later process is referred to as dissociative electron attachment.

In our work on ESD of anions formed by DEA from adsorbates on solid Kr and Xe we have found that the ESD yields can be significantly perturbed by the presence of the rare-gas substrates; specifically, the anion desorption yield often displays strong enhancement peaks superimposed on the normal ESD yield distributions. These peaks appear at incident electron energies slightly *below* the energies of the lowest exciton energies of the RGS. As will be discussed below, such narrow features are inconsistent with all mechanisms which involve elastic electron scattering in the RGS, or simple inelastic scattering of the incident electron in the solid to form excitons. We therefore postulate that the observed enhanced desorption yields are the result of a two-step process, initiated by the formation of anionic resonant states of the RGS, which is followed by the coupling of this resonance state of the RGS with the dissociative states of the adsorbed target species. The initial resonance state of the RGS binds the incident electron to the excitation, and therefore can be expected to follow the diffusive motion of the exciton as it traverses the rare-gas film. Such compound states are well documented in isolated electron–rare-gas atom collisions,[15–17] and have been predicted to exist in two-dimensional Xe layers.[18] Yet prior to our original study, they were unobserved in the RGS. Recent calculations by Munn, Mabbott, and Pope[19] support the existence of anionic excitations in molecular solids.

Whereas the study of electronically excited states of solids has traditionally focused on the preparation, dynamics, and eventual decay of the neutral exciton states, the present work will illustrate that an equally wide area of study is possible for the study of excited *anionic* states in the condensed phase of insulating materials. Like their electrically neutral counterparts, anionic excitations provide a mechanism for the quasielastic transport of energy in a medium[19] and for the coupling of this excitation to "impurity dopant" species contained in (or on) the medium. As will be shown, the resonant formation of these anion states provides an energetic specificity to the preparation of excited states which is normally not accessible during nonresonant inelastic electron-scattering events.

The format of this article is as follows. We first provide a summary of the dissociative electron attachment process. Experimental results for H_2O, C_2D_6, C_6D_6, and O_2 deposited on solid Ar, Kr, and Xe are presented afterwards. The evidence which leads us to conclude that the observed enhancements in the desorption yields are due to the resonant formation of anionic excitations in the RGS is given, followed by a theoretical explanation of the mechanism by which the core-excited anion resonance can move-hop within the RGS, and by which it couples to adsorbed "target" molecules. Finally, the possible application of these results is presented, along with directions for future work.

II. DISSOCIATIVE ELECTRON ATTACHMENT AT SURFACES

The DEA process, which for a polyatomic species ABC can be schematically written as

$$e^- + ABC \rightarrow (ABC)^- \rightarrow A^- + BC \ , \tag{1}$$

proceeds via a resonant anion state, here denoted $(ABC)^-$,which then dissociates to produce anionic and neutral fragments; it is implicitly assumed that A has a positive electron affinity and therefore the A^- species is stable with respect to electron autodetachment. The alternative decay channel for the $(ABC)^-$ resonance state into $A + BC^-$ may also be possible. If the energy release during a dissociation event at a solid-vacuum interface imparts sufficient kinetic energy to the anion fragment to induce desorption, the ESD yield can be monitored using a mass spectrometer positioned near the surface. For a given incident electron energy E_i, the kinetic energy in vacuum of the desorbing A^- fragment, E_k, is given by

$$E_k = (1-\beta)[E_i - E^* - E_b + EA(A) + E_{\rm pol}] - E_{\rm pol} \ , \tag{2}$$

where β is the ratio of the anion mass to the mass of the parent molecule, E^* is the internal energy of the fragment(s) following dissociation, E_b is the bond energy along the dissociation coordinate, $EA(A)$ is the electron affinity of the A fragment, and $E_{\rm pol}$ is the polarization barrier which must be overcome by the anion fragment during desorption. Above a few eV, the electronic structure of the $(ABC)^-$ transient anion state often corresponds to that for the attachment of an electron to a neutral excited "parent" state, i.e., $(ABC)^* + e^- \rightarrow (ABC)^{*-}$; if, as is usual in the case of DEA, the electron-excited state interaction potential supports a bound state of the electron, the excited anion state $(ABC)^{*-}$ will lie energetically *below* the energy of the neutral parent state, and the resonance is described as a core-excited Feshbach state (two-particle, one-hole). It is interesting to note that the dissociation of the lowest of these states is often the lowest-energy dissociation process observed for the parent species. As an example, the lowest-energy DEA process in gas-phase H_2O at 6.5 eV proceeds via the $^2B_1(1b_2)^2(3a_1)^2(1b_1)^1(3s{:}4a_1)^2$ anionic state,[20] while the lowest optically accessible excited state at 7.44 eV is the $^1B_1$ state,[21] with the electronic configuration $(1b_2)^2(3a_1)^2(1b_1)^1(3s{:}4a_1)^1$. It is also apparent from Eq. (2) that the DEA process at low incident energies will favor the desorption of light fragments (i.e., small β), even if the dynamics of the dissociation event favors the formation of more massive fragments. As an example, in the gas-phase DEA of H_2O, both H^- and O^-

anions are known to be formed with 6–8 eV electrons;[22,23] the thermodynamic onset for O^- *desorption* from a multilayer H_2O film, however, would be approximately 15 eV above the thermodynamic onset for H^- desorption.

Since the intermediate $(ABC)^{*-}$ state is resonant in nature, the dependence of the dissociation process on the incident electron energy can provide detailed information on ground-state to excited-(anionic)-state excitation probabilities, dissociative potential-energy surfaces, and dissociation branching probabilities; further information is available in the analysis of the kinetic energies of the desorbing fragments,[24] although the mass selectivity of the desorption process must be carefully considered in the DEA of adsorbed species. This technique allows us to determine the perturbations on the anion states and dissociation processes which are introduced by the condensed phase.[25,26]

III. EXPERIMENT

The apparatus used in these studies has been described previously[26,27] and is shown schematically in Fig. 1. The atomic and molecular species of interest are prepared and purified in an attached gas manifold and deposited under UHV conditions onto a clean 0.0075-in.-thick platinum foil substrate. This foil is supported on the cold tip of an APD-202 mechanical close-cycle refrigeration unit in order to obtain sample temperatures of ~17 K. The foil can be resistively heated to clean the surface and to desorb the condensed films. The metal surface and overlayer film are exposed to an electron beam produced by a home built hemispherical electron monochromator, with a central electron trajectory radius of 1.00 in., and operated at a relatively high pass energy of ~3.4 eV in order to increase the electron current delivered to the target. The output lens used to focus the electron beam onto the target consists of a double-zoom electrostatic system to maintain a relatively constant current vs energy profile for the electron flux across the energy region of interest. The angle of incidence for the electron beam was 70° from the surface normal. The present apparatus does not have provision to directly measure the energy distribution of the incident electron beam, although the design specifications predict[28] a distribution with a full width at half maximum (FWHM) of 85–95 meV; the energy resolution of similar devices in our laboratory (which directly measure the energy distribution using a second, identical, hemispherical analyzer) correspond closely to design specifications. The anion yield distributions are not found to change when the width of the energy distribution of the electron source was increased to ~135–140 meV. The electron beam current measured to a clean platinum target was typically 5×10^{-10} A. The electron energy scales of all results presented here are referenced such that 0.0 eV corresponds to the vacuum level (E_{vac}), using one of two methods. In the case of solid Xe and for the pure molecular solids, where the bottom of the conduction band is below the vacuum level, E_{vac} can be determined within ±0.3 eV by measuring the onset of current flow to the metal surface as the electron energy is slowly increased. In the case of Kr multilayer films, sharp structures are visible in the transmission curves (current to the metal as a function of electron energy) which can be correlated to those observed in previous studies,[29] where E_{vac} was determined more accurately than is possible in the present apparatus; the definition of E_{vac} for the Kr films is therefore believed to be accurate to within ±0.2 eV. Multilayer Ar films are somewhat anomalous in that V_0 lies 0.25 eV above E_{vac}. However, we have detected no changes in the onset of electron transmission when the platinum foil is covered by Ar films, and we therefore have taken the onset of the transmission through the Ar film to represent E_{vac}. The precision in peak positions for a given set of experiments is ±0.040 eV, for a given definition of E_{vac}. The lower-energy dispersion of the present electron monochromator provides more accuracy and reproducibility than was previously possible using a commercial electron gun; in particular, the observed resonant structures in the anion yield distributions of condensed H_2O are slightly lower in energy than previously reported.

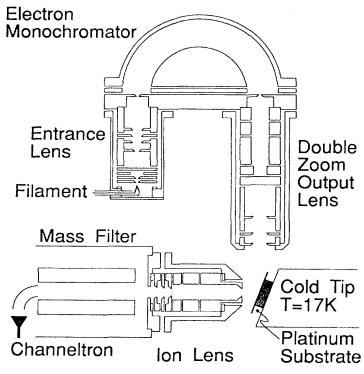

FIG. 1. Schematic view of the experimental apparatus. The components shown are housed in a conventional UHV chamber within two concentric layers of magnetic shielding.

The incident electron current was swept across the 0–15 eV energy range, where it induces DEA in adsorbed target species and leads to the formation of both adsorbed and desorbed anion fragments. A portion of the desorbing anion flux enters a Balzers quadrupole mass filter oriented at 20° from the surface normal, and the mass-selected anions are detected using a channeltron-type detector and conventional pulse-counting electronics. The electron monochromator, target assembly and mass filter are contained within a single UHV chamber, with typical base pressures of $\sim2\times10^{-10}$ Torr. The magnetic field in the experimental region and monochromator is reduced to ~10 mG by two layers of 0.010-in. magnetic shielding foil (Advanced Co-netics AD-78). In order to avoid surface/film charging by the incident electron beam and/or trapped charged particles, and to minimize contamination from residual background gases, most results shown here are the summation of the anion yields measured using 2–10 individual films. The typical duration of an experiment (between film deposition and deliberate evaporation from the platinum surface) was 5

TABLE I. Suppliers and purities of materials used in these experiments.

Gas	Supplier	Stated purity
Ar	Matheson	99.9995%
Kr	Matheson	99.995%
Xe	Matheson	99.995%
H_2O	In house	Double distilled, deionized
C_2D_6	MSD Isotopes	99%
C_6D_6	Aldrich	99.5%
O_2	Matheson	99.998%

min; under the conditions of the experiment, we expect that less than 0.03 of a monolayer (ML) of contamination from the background ambient gas pressure can deposit in this time, thus ensuring that the composition of the film is as-deposited. Deuterated adsorbates were often used to avoid interference by DEA of H_2O contamination, which could introduce the aforementioned H^- desorption for $E_i = 6-11$ eV.

The materials used in these experiments are listed in Table I, along with their stated purity and supplier. The liquids (H_2O and C_6D_6) were subject to several freeze-thaw cycles under vacuum in the vacuum manifold prior to use; all other materials were used as delivered. The thickness calibration of the deposited films has been previously described.[27] The absolute accuracy of this method is believed to be $\pm 50\%$; the relative precision of the deposition is estimated to be $\pm 10\%$. The accuracy of the deposition method for water is considerably lower, because of the slow desorption of the water from the walls of the dosing manifold onto the sample. In the case of water, the quoted coverage is estimated by comparison of the signal levels with that obtained from pure, multilayer water films deposited directly on the platinum foil.

IV. RESULTS AND DISCUSSION

The experimental results presented here are all obtained by monitoring the anion desorption flux while slowly varying the incident electron energy across the region of interest. The anion yield distributions for the pure molecular solids H_2O, C_2D_6, C_6D_6, and O_2 will be presented first, followed by the results obtained using RGS substrates. As would be expected from a comparison of such dissimilar adsorbates, the details of each system show significant variations, which will be discussed in turn; as will be seen, however, all systems show systematic behavior which can be understood in terms of a model which will be presented in Secs. VI and VII.

A. ESD from pure H_2O, C_2D_6, C_6D_6, and O_2 films

Figure 2 shows the H^- (D^-) anion desorption yields obtained from ~6-ML-thick-films of H_2O, C_2D_6, and C_6D_6, along with the O^- yield desorbing from 5 ML of O_2; all films were supported on clean platinum substrates. Each anion yield exhibits a single broad desorption peak in the 0–12 eV energy region; H^- (D^-) is by far the most abundant anion species detected from each of the hydrogen (deuterium) containing solids;[26,27] the resonant desorption of CD_2^- and CD_3^- was also observed from the pure, multilayer hydrocarbons, but with less than 1% of the intensity of the D^- signal.[27] O^- is always the dominant anion desorbed from films containing molecular oxygen.[25]

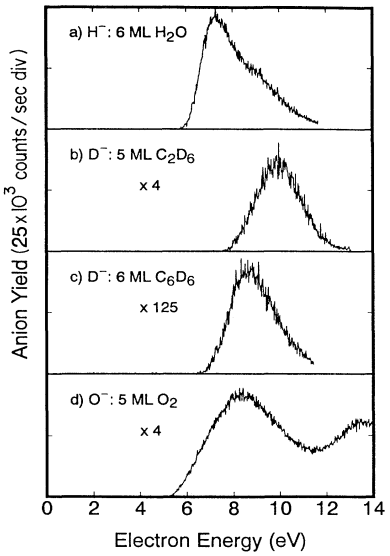

FIG. 2. Anion desorption yields for pure multilayer films of H_2O, C_2D_6, C_6D_6, and O_2 of the indicated thicknesses, deposited directly on the cryogenic platinum substrate. All energy scales are referenced to the vacuum level.

The H^- yield distribution for 6 ML of H_2O/Pt [Fig. 2(a)] shows an asymmetric profile with an onset at 5.5 eV, a maximum at 7.4 eV, and a broad tailing to higher E_i. The ESD of H^- from pure H_2O films has been discussed in detail previously.[26] The intense ESD maximum is believed to arise from the dissociation of the $^2B_1(1b_2)^2(3a_1)^2(1b_1)^2(3s{:}4a_1)^2$ anion state, while the desorption yield at higher incident energies is the result of the decay of the $^2A_1(1b_2)^2(3a_1)^1(1b_1)^2(3s{:}4a_1)^2$ anion state, in addition to some inelastic electron scattering in the multilayer H_2O film.[30] Like all anionic Rydberg-type excited states, these electronic configurations consist of two electrons orbiting the positive molecular-ion core at relatively large radii. The maxima of the DEA cross sections in gas-phase H_2O are at 6.5 and 8.6 eV, respectively.[20,22] A third DEA channel leading to H^- formation via the decay of the $^2B_2(1b_2)^1(3a_1)^2(1b_1)^2(3s{:}4a_1)^2$ anion state at 12.6 eV in the gas phase is not expected to be seen in the ESD data, since it generates only 0.2% of the anion yield produced by the main $^2B_1$ resonance.[20] The shifts of the $^2B_1$ and $^2A_1$ states to higher excitation energies in the condensed phase are believed to be the result of the Rydberg-orbital contributions to the electronic configurations of these excited states;[26] the first optical absorption of ice at 8.75 eV (Ref. 31) is similarly blueshifted from the 7.44-eV gas-phase absorption to the $^1B_1$ state.[21] The blueshift of condensed-phase Rydberg transitions (with respect to the gas phase) appears to be a general phenomena, while valence transitions tend to be

slightly redshifted in the condensed phase, due to increased polarization interactions of the excited state with the host matrix. In addition, it is possible that the excited $^2B_1$ state has significantly weaker hydrogen bonds between adjacent molecules than the $^1A_1$ ground state, due to the promotion of a $1b_1$ "lone pair" electron; this could contribute as much as 0.4 eV to the observed blue shifts found in condensed water. Recently, Bernheim and Wu[32] have reported that the H^- desorption yield from H_2O layers chemisorbed on aluminum substrates has a maximum anion yield at 5.8 eV; part of the discrepancy between the energies they report for the maximum anion yield and our own results for water films is due to their use of the midpoint of the leading edge of their transmission curve to define 0 eV, which is $\sim$1.4 V above the onset of transmission to the metal. The electronic structure and image potential acting on the transient anion species will also be significantly perturbed for the chemisorbed species, thus introducing additional energy shifts with respect to our physisorbed multilayer results. It is interesting to note that Bernheim's anion yield is much more symmetric than that seen here, suggesting that the second $^2A_1$ state does not contribute significantly to the anion field from chemisorbed H_2O/Al(111). The sensitivity of the $^2A_1$ state to the molecular environment will be discussed further in Sec. IV B. Although the shape of the DEA H^- yield profile shown here corresponds approximately to that seen in the gas phase,[22] it is important in the present context to verify that the observed yields correspond to the existence of a resonance state *at the energy of the incident electron.* In addition to the contributions from the decay of the $^2A_1$ anion state, two inelastic scattering processes could lead to the observed asymmetry of the ESD yield of Fig. 2(a). Inelastic electron scattering in the multilayer films prior to the DEA event could allow electrons with E_i above the resonance to induce dissociation, and therefore anomalously increase the *formation* of anions as E_i is increased; the enhanced desorption probability anticipated for fragments with higher kinetic energies could also anomalously increase the *detection* of anions at higher E_i. Both of these inhomogeneous processes could prevent the measured ESD profile from being proportional to the DEA probability. We cannot directly determine the magnitude of these inhomogeneous contributions in our results, however, we believe that they are relatively minor perturbations to the observed ESD yields. Paralleling the observations for the DEA of gas-phase water,[33] the width of the H^- ESD yield function is 30% broader than the D^- yield [measured under identical electron scattering conditions in a (D_2O+H_2O) film],[26] suggesting that inelastic scattering within the film does not significantly inhomogeneously broaden the nascent distribution; the lower intensity near $\sim$9 eV for D^- desorption with respect to H^- desorption also follows the gas-phase observations.[33] The maximum kinetic energy[26] for the desorbing H^- fragment from multilayer H_2O films has been shown to closely obey the conservation of energy expressed in Eq. (2); this would not be true if there were no state-to-state transitions and therefore we conclude that the $^2B_1$ and $^2A_1$ anion states can be prepared by a vertical Franck-Condon-type excitation from the ground state with electrons of 5.5–10.5 eV. As will be seen below, it is important that the observed ESD anion yields reflect the presence of dissociative anion *states* in the condensed phase.

The D^- desorption yield from multilayer C_2D_6 films [Fig. 2(b)] shows an onset near 7.5 eV and a maximum near 10 eV, as described previously.[27] The DEA desorption peak is unstructured and highly symmetric. The profiles and intensities of the H^- desorption yields are remarkably similar for all *n* alkanes larger than methane.[27] The DEA profile for gas-phase ethane measured by Dorman[34] has a single, unstructured maximum for H^- formation at 9.5 eV, with a FWHM of $\sim$2 eV; onsets for anion formation were not reported. Unlike the case for H_2O, the DEA processes in ethane vapor are poorly characterized, and no state-specific investigations for the transient anion states involved have been published. We will attempt to characterize the electronic structure of the dissociative $(C_2D_6)^{*-}$ resonance state by comparing the DEA results with the gas- and condensed-phase optical absorption spectra for ethane, assuming that the optically accessible dissociative states are related to the parent states of the dissociative anion state. The lowest optical absorption in gas-phase ethane has an onset near 7.9 eV and a broad maximum of 9.4 eV.[35,36] Buenker and Peyerimhoff[37] have calculated that the first excited *valence* state of ethane should be $\sim$15.5 eV above the ground state, i.e., $\sim$6 eV above the first observed transition energy; Sandorfy[38] has concluded that the lowest optical absorptions of *all* acyclic paraffins therefore correspond to electron promotion from the $1e_g$ or $3a_{1g}$ molecular orbital to the 3*s* or 3*p Rydberg* orbital. The triplet states of the *n* alkanes are expected to be only slightly lower in energy than the optically accessible singlets.[36] The optical absorption spectra of solid and liquid ethane[11] are similar to the gas-phase absorption spectrum, and it is believed that the electronic structures of the excited states in the condensed phase are closely related to those of the gas phase. Jordan and Burrow[39] have determined that no transient anion states exist for the *n* alkanes below 5 eV, and we may therefore assume that the anion yields reported here and by Dorman[34] correspond to the dissociation from the lowest anionic state of ethane. If the electronic structure of the lowest transient anion state of $(C_2D_6)^{*-}$ is related to the electronic structure of the lowest optically prepared excited state of $(C_2D_6)^*$ (i.e., the optically prepared state is related to the parent of the anion resonance state), we would conclude that the transient anion state would consist of a vacancy of the $1e_g$ or $3a_{1g}$ molecular orbital, with two electrons in the Rydberg-like 3*s* or 3*p* orbital. It is extremely unlikely that the proposed valence state calculated to be near 15 eV (Ref. 37) (or its nearby triplet counterpart) would be the parent of the anion resonance state since they would be separated by over 7 eV in the gas phase.

The D^- desorption yield from multilayer C_6D_6 films [Fig. 2(c)] has an onset at 6.6 eV and a single maximum at 8.9 eV; the isotropic purity of the C_6D_6 was verified by the absence of an H^- desorption yield from freshly deposited C_6D_6 films. To the best of our knowledge, these are the first published D^- (or H^-) yield distributions

from gas-phase or adsorbed benzene. The ESD yield has a FWHM of ~3 eV, and is slightly asymmetric, suggesting the presence of overlapping dissociative anion states (as proposed for ESD from pure H_2O films), or perhaps indicating the presence of inelastic-scattering processes which distort the measured ESD profile from the nascent D^- distribution. Fenzlaff and Illenberger[40] have detected the formation of $C_2H_2^-$ and $C_6H_5^-$ via the DEA process in benzene vapor, with anion yield maxima at ~9 and 8 eV, respectively, and appearance potentials of ~6 and 7 eV, respectively. The width of their $C_6H_5^-$ anion yield is clearly less than that of the $C_2H_2^-$ profile. von Trepka and Neuert[41] have reported 15 anion fragments to be formed in the DEA of gas-phase benzene, including a strong H^- channel with an appearance potential of 7.9 eV; they reported that the appearance potentials for the various fragmentation channels span a range of 4.7 eV, although no explicit anion yield curves were shown for the benzene results. In the case of condensed-phase benzene, there is insufficient kinetic energy release to desorb a $C_6D_5^-$ fragment; the formation of $C_6D_5^-$ with sufficient kinetic energy to overcome the ~1-eV polarization barrier of the surface, and hence desorb, would require an energy release of ~42 eV during dissociation, according to Eq. (2).

In an effort to characterize the nature of the electronic states which give rise to the DEA of benzene, we can again attempt to correlate the DEA data with the optical absorption data, in order to determine the parentage of the resonance state. The optical spectrum for gas-phase benzene below ~7.5 eV is characterized by three strong valence absorptions ($^1B_{2u}$, $^1B_{1u}$, and $^1E_{1u}$ with maxima near 5.9, 6.2, and 7.0 eV, respectively).[36,42,43] Above this spectral region, there are at least four series of sharp Rydberg transitions leading to the first and second ionization limits (9.27 and 11.49 eV, respectively) which are superimposed on a broad quasicontinuum of valence absorptions. Electron energy-loss spectroscopy (EELS) of gas-phase benzene[43] has detected four transitions to triplet valence states ($^3B_{1u}$, $^3E_{1u}$, $^3B_{2u}$, and $^3E_{2g}$, with maxima at 3.9, 4.7, 5.6, and 6.2 eV, respectively), as well as several series of optically forbidden Rydberg transitions above 8 eV. The EELS spectra of benzene films (and benzene in Xe matrices) measured by Sanche and Michaud[44] show the maxima of the transitions to excited singlet and triplet valence states to be within 0.3 eV of the gas-phase transition energies; no specific Rydberg transitions were observed in their work. Katz *et al.*[45] have observed the lowest optical Rydberg transitions of benzene to be blue shifted by 0.2–0.4 eV from their gas-phase energies when dissolved in the RGS, although subsequent work by Angus and Morris[46] failed to observe one of the C_6D_6/Xe Rydberg absorptions at 7.5 eV. Due to the congestion of electronic states in the 5–12 eV region for benzene, it is not yet possible to precisely identify the parentage of the observed DEA resonance(s); it is probable, however, that the Rydberg contributions can only dominate the resonance states which are at least 8 eV above the ground state. We expect that the density of Rydberg-derived states will increase as the ionization limits are approached, since the gas-phase Rydberg series converge to these asymptotes.

Azria and Schulz[47] have detected seven anion resonance states of $(C_6H_6)^-$ below 12 eV using EELS; all decay into vibrational excitations of the neutral molecule, while the broad 8 eV *g* resonance also leads to DEA. Allan[48] has suggested that the *g* resonance state may be a $^2E_{1u}\sigma^*$ state, with both the promoted and incident electrons temporarily occupying the σ^* valence orbital. Alternatively, Robin[36] has suggested that two Rydberg states (two electrons in 3*s* or 3*p* orbitals, bound to a core excitation from the $e_{2g}\sigma$ molecular orbital) could be better candidates for the resonant states which lead to DEA, since the widths of the DEA anion yields of Fenzlaff and Illenberger[40] are approximately 25% narrower than the resonances reported by Allan[48] or by Azria and Schulz.[47] In view of the very different anion yield distributions reported for the $C_6H_5^-$ and $C_2H_2^-$ fragmentation channels,[40] and the different onsets for the various fragmentation channels,[40,41] it is almost certain that several dissociative anion states overlap in the 7–10 eV region; from the observations based on the optical data for benzene[36] it is expected that DEA events which occur at higher incident electron energies are more likely to involve Rydberg states than those at lower energies.

Figure 2(d) presents the O^- desorption yields from pure multilayer oxygen films; heavier anions are also observed to desorb in lower yields,[25] but will not be discussed here. The dominant desorption feature is the broad, asymmetric peak near 7–9 eV, with a weaker desorption signal at ~13 eV, followed by a gradually increasing dipolar dissociation process above 15 eV. The gas-phase DEA of O_2 to form O^- proceeds exclusively via the $^2\Pi_u$ anion resonance at 6.7 eV;[49] this resonance state has the electronic configuration $(2\sigma_g)^2(1\pi_u)^3(1\pi_g^*)^4$, with both the incident electron and the promoted $1\pi_u$ electron occupying the $1\pi_g^*$ valence molecular orbital. The large width of the ESD yield near 6–9 eV is a convolution of the $^2\Pi_u$ and $^2\Sigma_g^+$ states, while the feature near 13 eV is assigned to a $^3\Sigma_g^- \rightarrow {}^2\Sigma_u^+$ transition in the solid;[50,51] $\Sigma^- \rightarrow \Sigma^+$ transitions are symmetry forbidden in the gas phase, but allowed in solid O_2 and O_2 clusters[52] because of the relaxation of the cylindrical symmetry in these high-density environments. A similar relaxation of this selection rule is found in the optical spectra of condensed-phase oxygen.[53,54] All available data suggests that the states involved in the DEA of gas-phase and condensed-phase O_2 are exclusively within the valence manifold.

B. ESD from H_2O/Ar, H_2O/Kr, and H_2O/Xe films

The preliminary results for the H_2O/Kr and H_2O/Xe systems were the object of our earlier work.[55] The H^- ESD yields shown in Fig. 3(a) shows the effect of depositing approximately 0.1 ML of H_2O on 20 ML of solid Kr. It is unlikely that the H_2O exists in monomeric form on the RGS at these coverages, due to its strong hydrogen-bonding interactions with adjacent H_2O molecules.[56] The distinctive difference which is introduced by the RGS substrate is a new, narrow ESD peak at 9.6–9.7 eV. This new peak is clearly absent in the pure multilayer H_2O

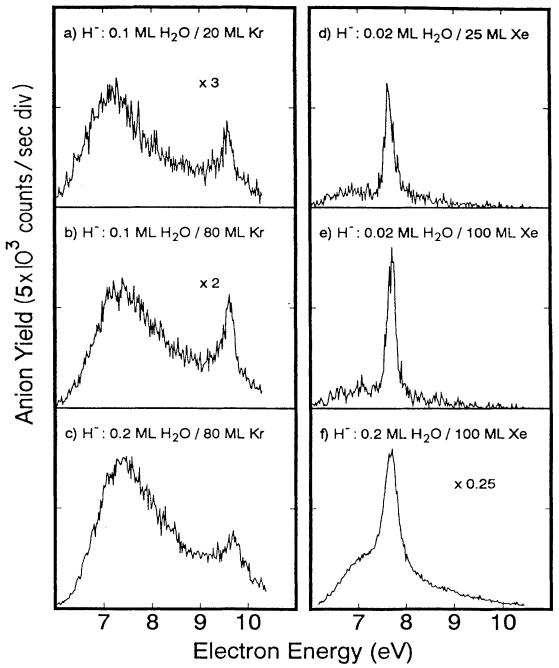

FIG. 3. H^- desorption yields for submonolayer H_2O deposited on rare-gas films of the indicated thickness. The data of (a)–(c) were obtained using Kr substrates, while the data of (d)–(f) were obtained using Xe substrates. The quantities of adsorbed H_2O are estimated by comparison with the signal levels for pure, multilayer H_2O films.

film results of Fig. 2(a), and has no counterpart in the DEA of gas phase,[20,22] cluster phase,[57,58] or condensed phase H_2O.[26] The relative contribution of this new peak becomes more apparent as thickness of the RGS is increased to 80 ML [Fig. 3(b)]. In the discussions that follow, we shall refer to the unenhanced contributions to the total anion yield as the "direct" contributions, and focus our attention on the narrow enhancement of the desorption yields. Figure 3(c) shows the effect of increasing the quantity of water deposited on the 80-ML Kr substrate; the direct contributions have increased because of the increased surface coverage, and the enhanced peak is seen to broaden significantly. More importantly, it is apparent that the relative contribution of the enhancement with respect to the direct contributions decreases as the coverage of H_2O is increased, even when this coverage is far less than a complete monolayer, although the probable aggregation of H_2O on the RGS implies that the dose-based coverage is only approximately related to the actual microscopic isolation for the target molecules on the RGS. We have previously demonstrated that the position of the enhancement is not sensitive to the incident angle of the electron beam.[55]

Similar results were obtained using Xe spacer layers; Figs. 3(d)–3(f) show the anion yield distributions for $\sim$0.02 ML of H_2O supported on 25 and 100 ML of Xe, and with an increased coverage of the 100 ML of Xe by water. An enhanced anion desorption is detected at 7.7 ± 0.1 eV, which rises above the direct anion yield distribution from the adsorbed H_2O.

Aside from the narrow signal enhancement, the profiles of the direct contributions from the submonolayer H_2O/Kr and submonolayer H_2O/Xe films are remarkably similar to those from pure multilayer H_2O films. To demonstrate the relationship between the anion yields from pure and rare-gas supported H_2O more clearly, Fig. 4 presents the same data presented in Figs. 3(a)–3(f), normalized by the smoothed H^- yields from pure H_2O films [e.g., the signal of Fig. 2(a)]. This manipulation emphasizes the fact that the observed narrow peaks are *enhancements* of the DEA probability within a particular energy region; subtracting the direct contributions would imply that the two portions of the total signal were uncorrelated. In the absence of an interaction with the RGS, this ratio would be a relatively flat "base line," which would indicate the quantity of water adsorbed onto the RGS; a base-line ratio of 1.0 need not correspond to 1.0 ML of H_2O, because of the possibility of anion desorption from the second and third layers of the multilayer data of Fig. 2(a), as well as the possibility that the absolute anion yield is sensitive to the anion-platinum separation. The effects of the interaction with the RGS are seen as approximately Gaussian-shaped enhancements near 9.6–9.7 and 7.7 eV on the Kr and Xe substrates, respectively. The heavy line drawn through each set of experimental data is the fit[59] to the formula

$$\text{fit}(E_i) = \text{Amp}^*\exp[-(E_i-E_0)^2/w^2]+B \ , \qquad (3)$$

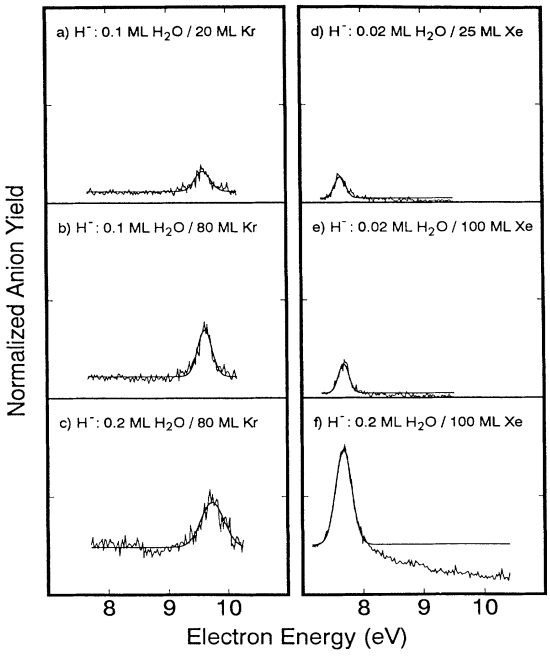

FIG. 4. Ratio of the data of Figs. 3(a)–3(f) to the data of Fig. 2(a); the full scale of each frame is 1.0. The solid line drawn through each data set represents the best fit of a Gaussian line shape superimposed on a constant background, as described in the text.

where E_0 is the center of the enhancement, w is the $1/e$ width of the feature, and B represents the base line. This functional form was chosen simply as a convenient method to quantify the results; Lorentzian line shapes fit the data less satisfactorily than the Gaussian line shape. Above ~ 10 eV, the base lines of the ratio plots are seen to decrease slightly; as will be discussed below, this could be due to a reduction in the inelastic electron scattering in the submonolayer H_2O films or due to a continuing interaction between the anion states of H_2O with the RGS.

Although the enhancement for the H_2O/Kr ratio data is well described by the Gaussian line shape, there exists a slight residual broadening at the base of the enhancement using 3–10 ML of Kr. The reason for this is not clear, and it is not found for any of the other gases used as adsorbates in this study. It should be noted, however, that the energy of the enhancement corresponds very closely to the anticipated energy of the $^2A_1$ anion state in condensed water,[26] and it is possible that the enhancement process for the $^2A_1$ state is more sensitive to the local environment than is the $^2B_1$ state. The FWHM of the Gaussian line shape is approximately 0.23–0.3 eV; the FWHM of the electron energy distribution from the electron monochromator induces only $\sim$20-meV broadening to the enhancement feature. Even without considering the deconvolution of the experimental resolution, the observed enhancements are the narrowest features reported to date using ESD. Unlike the results for H_2O/Kr, the width of the enhancement observed with Xe spacers does not decrease as the rare gas thickness is increased, and no broadening is observed at the base of the enhancement.

The amplitude of these features can be used to quantify the enhancement under a specific set of film conditions; the ratio of the amplitude to the constant base line is proportional to the amplitude *per unit coverage,* or the gain of the DEA probability induced by the RGS. Figure 5 displays the gain as a function of the thickness δl of the RGS layers; these data were taken in the limit of extremely low coverages of the RGS by H_2O, with base-line ratios always being less than 0.1. The lines drawn through the data represent the best fit to the functional form

$$\text{gain}(\delta l)=G_\infty\{1-\exp(-\delta l/L_0)\}\ , \tag{4}$$

where G_∞ is the gain in the limit of an infinitely thick rare-gas substrate, and L_0 defines the length scale by which the experimental gain approaches this limit. The fit parameters for the H_2O/Kr system were $G_\infty=3.1$, $L_0=19.8$ ML; the fit parameters for the H_2O/Xe system were $G_\infty=7.9$, $L_0=21.7$ ML. The Xe substrates therefore enhance the anion yields more effectively than do the Kr substrates. These limits are only obtained with rather thick layers of the RGS. From our present understanding of DEA on surfaces,[14,60] we would expect that as the distance between the transient $(H_2O)^{*-}$ anion and the metal substrate is increased, the desorption yield of H^- will increase due to the reduced quenching of the excited $^2B_1$ and $^2A_1$ anion states by the image forces of the platinum support. This would be manifested as an increase in both the direct and the enhanced contributions to the total signal such that the ratio of the enhancement to the base line (i.e., the gain) will not be sensitive to this effect. Furthermore, the influence of the metal should be small beyond separations corresponding to ~ 10 ML.[61,62] The observed increase of the gain with increasing thickness of the RGS can arise from two interrelated processes. If the origin of the enhancement is in the bulk of the Kr and Xe RGS, rather than selectively at the surface, the thickness dependence of the yield would be the result of a transport mechanism from the bulk to the surface, with characteristic "diffusion" lengths of the order of 20 ML. Alternatively, the mechanism of the enhancement may be extremely sensitive to the presence of the metal substrate; in this case, the observed thickness dependence would reflect the reduced quenching of the intermediate excited states of the solid as the average distance to the metal is increased. Both of these processes involve transport mechanisms in the RGS.

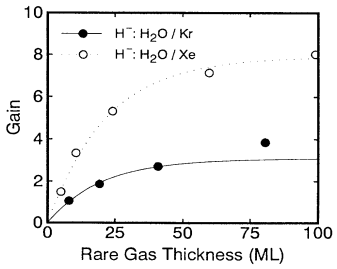

FIG. 5. Experimental gain of the H^- desorption yield from submonolayer H_2O which is induced by the Kr and Xe substrates (solid and open circles, respectively), shown as a function of the rare-gas thickness δl in monolayers. The lines drawn through the experimental points are the best fit to the functional form gain $(\delta l)=G_\infty\{1-\exp(-\delta l/L_0)\}$, as described in the text.

No enhanced anion yields were detected for submonolayer H_2O supported on thick Ar substrates. It is probable that much of the rather weak direct ESD yields above $E_i\sim 10$ eV from pure multilayer H_2O films [Fig. 2(a)] are produced by inelastic electron scattering in the film prior to DEA, and therefore the true DEA cross section at these incident electron energies could be negligible. Alternatively, the coupling between the initial excitation of the Ar RGS and the target molecules could be significantly weaker than for the Kr and Xe substrates.

Because of the difficulty of depositing a precise known submonolayer quantity of H_2O onto the rare-gas solids and the unknown degree of aggregation on the RGS, it was not possible to perform a systematic investigation of the sensitivity of the enhancement to the quantity of H_2O deposited onto a fixed thickness of Kr or Xe. Qualitatively, the enhancement is seen to broaden as more water is deposited, and the significance of the enhancement with respect to the direct signal is found to decrease until it is lost in the anion yield distribution of the pure H_2O. The gain is found to *decrease* as more H_2O is deposited, even in the submonolayer H_2O regime. This point will be expanded upon in more detail in presenting the C_2D_6 re-

sults, since the *n* alkanes are amenable to more precise control during deposition than is water vapor.

C. C_2D_6/Ar, C_2D_6/Kr, and C_2D_6/Xe

Figure 6 presents the D^- ESD yields obtained for submonolayer C_2D_6 adsorbed on Ar, Kr, and Xe RGS films of 17, 80, and 50 ML thickness, respectively. The direct contributions to the total desorption signal are visible for each substrate and are consistent with estimates based on the known coverage of the RGS by the C_2D_6.[27] The data for C_2D_6/Ar [Fig. 6(a)] show a weakly enhanced desorption from $E_i = 11.5-11.7$ eV. The direct contribution for the C_2D_6/Ar system has a maximum near 9.7–9.9 eV, with a FWHM of approximately 2.3 eV; it is therefore similar to the profile of the anion desorption yield from pure, multilayer C_2D_6 [Fig. 2(b)]. The magnitude of the enhancement using Ar substrates is difficult to quantify because of its low intensity, but it was approximately 30–50 % of the direct contributions (at the energy of the enhancement) in the limit of low C_2D_6 coverages and represents a gain of only 0.3–0.5. This is at least five times less than observed with the Kr or Xe substrates. We could not detect any significant improvements in the enhancement by adjusting the thickness of the rare-gas substrate. The optimum surface coverage of C_2D_6 for the detection of the weak feature appears to be ~0.1 ML; larger coverages tended to completely obscure the enhancement with the direct contributions, while lower coverages made detection extremely difficult. Following the reasoning outlined above, the insensitivity of the gain to the thickness of the Ar RGS could indicate that the transport mechanisms are less effective in solid Ar than found using Kr or Xe substrates. Figure 6(b) presents the D^- anion yields from the C_2D_6 adsorbed on a Kr substrate. Although the position of the enhancement at 9.6–9.7 eV is clear, the position of the maximum signal for the direct contributions is uncertain since the pure multilayer films have a maximum very close to the observed enhancements which dominate the yield functions. It is obvious, however, that the direct anion yield is asymmetric around the enhancement, with significantly less signal above the enhanced peak. This can either reflect a shift of the direct DEA profile to lower E_i when supported on the Kr substrate or a reduction of the direct contributions for E_i above the main enhancement. The onset for the D^- desorption signal from the Kr substrate is similar to that from the pure C_2D_6 films. Lacking information to the contrary, and based on our observations using Ar substrates, we assume that the multilayer results are an adequate model for the direct contributions on the Kr (or Xe) substrates, and that the observed asymmetry reflects a quenching of the direct contributions at incident energies above the energy of the enhanced desorption yield. In considering the results for C_2D_6/Xe, we observe the narrow enhancement near 7.7 eV, and that the intensity of the direct contributions for E_i above the main enhancement is again significantly lower than that expected on the basis of the pure multilayer results; at the energy of the maximum anion yield for the pure C_2D_6 (9.9 eV), there is almost no detectable signal using the Xe substrates. These results indicate that in the case of C_2D_6 target species, the intensity of the direct contribution is suppressed for E_i above the enhanced yields. It should be noted that in the case of submonolayer O_2/Ar, O_2/Kr, and O_2/Xe,[25] the onsets for the O^- desorption are all within 0.25 eV for the different RGS, yet the maxima of the desorption yield can vary by as much as 0.75 eV; the assumption of direct contributions which are unaffected by the RGS should therefore be considered as somewhat tentative. The onset of the enhancement observed using Xe substrates occurs within 0.2 eV of the onset for the direct contributions; as will be shown below, this indicates that the transport mechanism which leads to the enhanced yields must be elastic or quasielastic. The shape and intensity of the D^- desorption yield from C_2D_6/Xe was not sensitive to the temperature of the Xe deposition in the range of 30–50 K.

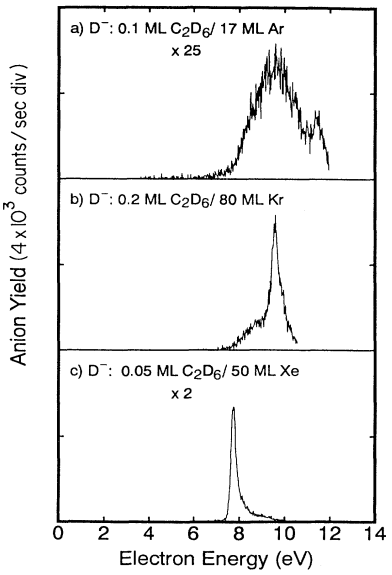

FIG. 6. D^- desorption yield for submonolayer C_2D_6 supported on Ar, Kr, and Xe substrates of the indicated thicknesses. Above the energy of the enhancement feature, the anion desorption yield is sharply reduced, as can be seen by comparison with Fig. 2(b).

We have also measured the kinetic-energy distributions of the desorbing D^- flux from C_2D_6/Kr for $E_i = 8.5-11.0$ eV. As the incident energy is increased across the energy of the enhancement feature, there is no significant change in the shape of the distribution, except for the continuous progression to higher maximum kinetic energies, as expected on the basis of the conservation of energy during the dissociation process, i.e., Eq. (2). The absence of singularities or other anomalous structures in the kinetic-energy distributions suggests that the dissociation and desorption mechanisms are not modified in the energy range corresponding to the enhancement. The enhanced anion yields are linearly dependent on the incident electron current, as are the direct contributions.

The C_2D_6/Kr and C_2D_6/Xe data were quantified using

the normalization procedure described above for the H_2O/Kr and H_2O/Xe data, and display similar trends. We have measured the effect of depositing increasing quantities of C_2D_6 on 40-ML-thick Kr substrates; the gain (Fig. 7) is a rapidly decreasing function of coverage, even in the very low coverage regime; it is unlikely that the ethane is aggregating on the surface. The highest gain of ~6–7 for Kr substrates is found in the limit of zero coverage, and is twice that found in the case of the H_2O/Kr data. Since it is extremely difficult to collect data at very low coverages, we have quantified the gain as a function of substrate thickness δl using a C_2D_6 coverage of ~0.2 ML; these data are summarized in Fig. 8 for the Kr substrate. The line drawn through the data describes the saturation behavior of the thickness trends, as described above for the H_2O results; the best-fit parameters were $G_\infty = 1.7$, $L_0 = 18.5$ ML. Due to the very low intensity of the direct contributions at the energy of the Xe-induced enhancement, it is impossible to calculate the gain for the C_2D_6/Xe system with precision; however, it is apparent from Fig. 6 that Xe is more effective than Kr in enhancing the DEA probability. In the limit of very low C_2D_6 coverages, both are found to enhance the yields from adsorbed C_2D_6 more effectively than from adsorbed H_2O. We speculate that the lower gains found with H_2O are due to clustering of the water on the RGS such that the true local coverage of H_2O was larger than indicated by the magnitude of the direct contributions. In general, the gain of the enhancement is seen to follow the Ar $\ll$ Kr < Xe sequence.

D. C_6D_6/Kr and C_6D_6/Xe

Figures 9(a) and 9(b) show the D^- anion yields measured for 0.25 ML of deuterated benzene deposited on 40 and 60 ML of Kr and Xe, respectively. The overall signal levels are very low, as also seen in the pure benzene results of Fig. 2(c); this required the summation of as many as 48 scans to measure a single anion yield distribution. The D^- anion yields observed with Kr substrates show the familiar enhancement of the anion yields, at $E_i = 9.5$ eV; the 0.38 eV width of the enhancement feature is significantly greater than observed for the H_2O or C_2D_6 adsorbates. It is probable that the benzene films

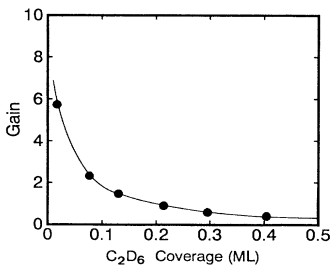

FIG. 7. Experimental gain of the D^- desorption yield from submonolayer C_2D_6 on 40 monolayers of Kr, shown as a function of the quantity of C_2D_6 deposited. The line is drawn to guide the eye.

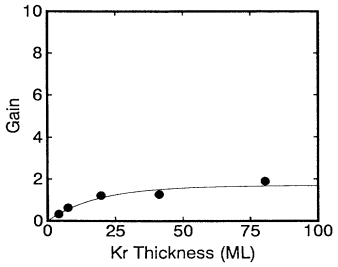

FIG. 8. Experimental gain of the D^- desorption yield from 0.2 monolayers of C_2D_6 on Kr substrates, shown as a function of the Kr thickness δl in monolayers. The line drawn through the points is the best fit to the functional form gain $(\delta l) = G_\infty\{1-\exp(-\delta l/L_0)\}$, as described in the text.

were rapidly acquiring excess surface charges during the ESD experiment, which would explain both the large widths of the enhanced desorption yields and the slight shift of the maximum from that observed using H_2O or C_2D_6. Unlike the results for the H_2O and C_2D_6 adsorbates, the enhanced anion yields from the C_6D_6 on Kr were not found to be sensitive to the C_6D_6 coverage below ~0.5 ML. The sensitivity to the thickness of the Kr RGS was also less pronounced than found with adsorbed H_2O and C_2D_6.

The desorption yields obtained using Xe spacer layers [Fig. 9(b)] are particularly interesting in that the total anion yield distribution is remarkably similar to that of the pure multilayer films of Fig. 2(c). No enhancements are visible in the ESD yield near 7.5–8.0 eV. This negative result was found for all thicknesses of the Xe substrate and all overlayer coverages. To verify that the apparatus and experimental conditions were consistent with previous studies, H_2O from the residual background pressure was allowed to deposit on the C_6D_6/Xe films; the enhanced H^- peak arising from the coadsorbed H_2O was

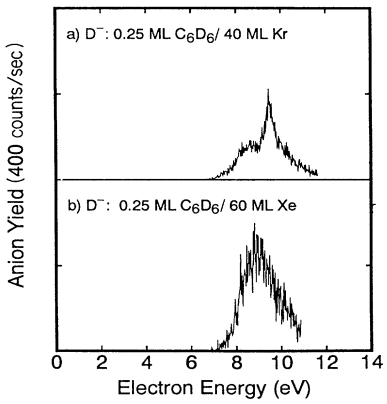

FIG. 9. D^- desorption yield for submonolayer C_6D_6 supported on Kr and Xe substrates. Unlike the C_6D_6 data, the C_6D_6/Xe results show no enhancement features, regardless of the thickness of the Xe substrate or of the quantity of adsorbed C_6D_6.

clearly seen, while no enhanced D^- from C_6D_6 was found.

E. O_2/Ar, O_2/Kr, and O_2/Xe

Previous publications have reported the anion desorption yields from oxygen deposited on Ar, Kr, and Xe RGS;[25] data measured with the new higher-resolution electron source are shown in Figs. 10(a)–10(c). The O^- desorption yield for each system shows a single, dominant peak near 6–7 eV due to the decay of the $^2\Pi_u$ state of O_2^- into the DEA channel. The contribution of the two "forbidden" $^3\Sigma_g^- \rightarrow {}^2\Sigma_{g,u}^+$ DEA processes to the overall desorption yield is essentially zero when the oxygen is supported on the RGS films in submonolayer coverages, which is consistent with the proposed mechanism which requires breaking the cylindrical symmetry of the adsorbed O_2 by the presence of adjacent O_2 molecules. Even though the O^- signal is strong (and therefore easier to quantify at low O_2 coverages), *there are no enhanced anion desorption features observed for O_2 supported on any of the RGS substrates, regardless of the O_2 coverage.* In the case of the Ar substrate, this is perhaps not surprising since the intensity of the direct desorption yield in the 11–12 eV region is very weak. However, in the case of the Kr and Xe substrates, there is sufficient direct intensity near $E_i = 9.7$ and 7.7 eV to expect that the enhanced desorption yields could be evident. The complete absence of enhanced yields under conditions which lead to their observation using other target species indicates that the O_2 molecule does not support the mechanism of the yield enhancements.

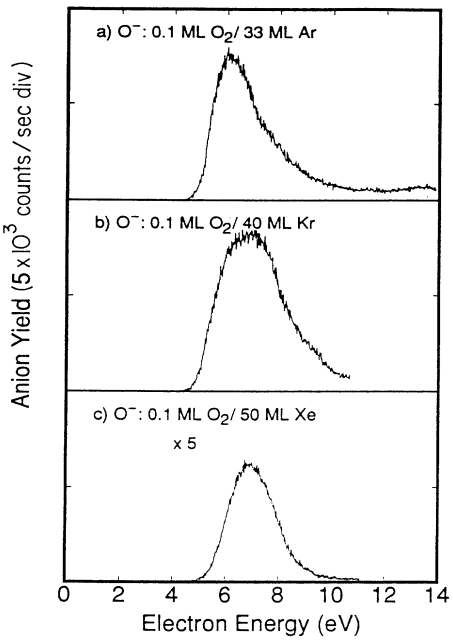

FIG. 10. O^- desorption yield from submonolayer O_2 on Ar, Kr, and Xe substrates. No enhancement features are observed, regardless of the substrate thickness or of the quantity of adsorbed O_2.

V. SUMMARY OF ESD RESULTS USING RGS SUBSTRATES

The results presented above are summarized here.

(a) The enhanced anion yields are systematically observed near 7.7, 9.7, and 11.6 eV for Xe, Kr and Ar substrates, respectively; these energies are not strongly sensitive to the thickness of the RGS, the identity of the target molecules, or the angle of incidence for the electron beam.

(b) The line shapes of the enhanced yields are well described as Gaussian, with widths (FWHM) of approximately 0.7, 0.3, and 0.2 eV for Ar, Kr, and Xe substrates, respectively. The widths are not instrumentally limited and do not depend strongly on the thickness of the RGS substrates, except in the case of H^- from H_2O/Kr, which decreases with increasing RGS thickness.

(c) The absolute intensity of the enhanced yields increases with increasing coverage of the RGS by the target species, but the enhancement per target molecule (i.e., the gain) decreases as the coverage is increased. The gain of the enhancement increases according to Eq. (4) as the thickness of the RGS is increased. The magnitude of the direct signal is insensitive to the thickness of the RGS.

(d) The anion desorption yield is linearly proportional to the incident electron current for both the direct and enhanced signals. The kinetic energy of the desorbing anion fragments show no anomalous changes as E_i is swept across the energy of the enhancement feature.

(e) The enhancement occurs in the DEA yields which arise by the decay of core-excited *Rydberg* resonance states such as the $^2B_1$ state of H_2O^-, but not in the DEA yields produced by the decay of core-excited *valence* resonance states such as the $^2\Pi_u$ state of O_2^-. Adsorbates that have overlapping valence and Rydberg bands (e.g., $C_6D_6^-$) show the enhanced desorption yields only if there exist Rydberg transitions which can be associated to DEA states at the anticipated energy of the enhancement.

(f) For target species which can be expected to show enhanced yields for all three RGS substrates (e.g., C_2D_6), the gain is in the order of Xe > Kr >> Ar.

(g) Above the energy of enhancement, attenuation (or quenching) of the direct signal is observed for Xe and Kr substrates. The magnitude of the attenuation is in the order Xe > Kr >> Ar.

The most important observations which can be made concerning the nature of the initial excitation are that the incident electron energies corresponding to the enhancements are below the energy required to form bulk or surface excitons of the RGS, and that the widths of the enhancements are extremely narrow with respect to the excitation functions for exciton formation using electron impact.[13,63] The lowest optically accessible excitons of the RGS are the $\Gamma_{\frac{3}{2}} n = 1$ surface excitons at 11.8, 9.95, and 8.21 eV for Ar, Kr, and Xe, respectively;[64] the corresponding bulk exciton bands are at 12.1, 10.17, and 8.37 eV, respectively. In the case of bulk exciton formation by electron impact, the excitation functions for exciton formation will be shifted by a quantity V_0. This shift is introduced by the requirement that the inelastically scat-

tered electron must propagate in a band of the film following the excitation of the solid; the lowest available band will be the conduction band of the RGS. In the case of surface excitons, the electron either leaves the film following the excitation such that the construction and energy of the conduction band need not be relevant, or it couples with the surface band structure, in which case its energy at the threshold for the enhancement must lie between the vacuum level and V_0. However, the sensitivity of the enhancement to the thickness of the RGS indicates that the initial energy deposition need not take place at the surface. The best available estimates for V_0 in the solid RGS are $+0.25$, -0.4, and -0.5 eV for Ar, Kr, and Xe,[64] respectively, measured with respect to E_{vac}. The estimated threshold energies which could lead to exciton formation by electron impact in the bulk are $E_i = 12.35$, 9.77, and 7.87 eV for Ar, Kr, and Xe, respectively. These energies are sufficiently close to the experimental energies of the yield enhancements for us to consider if exciton formation could lead to enhanced dissociation yields. The conventional decay channel for the excitons of the RGS is by photon emission,[65] but, of course, the DEA process cannot be induced by simple optical excitation or by the transfer of energy from a neutral species. It is known that desorption of ground-state species from the RGS can be caused by relaxation of excitons,[63] and it may be postulated that the enhanced anion yields observed in the present experiments reflect an increased *desorption* rate of existing anion fragments trapped at the surface,[66,67] rather than an enhanced *dissociation* yield. If this "two-step hypothesis" was correct, we would anticipate that (a) those adsorbates which produce large quantities of adsorbed anion fragments, such as O_2,[68] would also produce large enhanced desorption yields, (b) a given adsorbate would have little sensitivity to the identity of the RGS, (c) the magnitude of the enhancement would be quadratically dependent on the incident current, and (d) the profile of the desorption yield would correspond to the profile for exciton creation by electron impact. The results for adsorbed O_2 and C_6D_6 are clearly contrary to prediction (a) and (b), respectively. The first-order dependence of the anion yields on the incident electron current rules out (c), as well as all exciton-exciton annihilation processes, which have been reported for molecular solids.[69–71] The excitation functions for exciton creation in the RGS during electron impact are known to be several eV in width due to the nonresonant nature of the inelastic-scattering event. Coletti, Debever, and Zimmerer[63] have measured the total luminescence yield of solid Ar during exposure to low-energy electrons and found that the onset of photon emission corresponds closely to that of exciton formation; in the range of $E_i = 0$–50 eV, there were no structures in the luminescence yield with FWHM less than 5 eV, showing again that the exciton formation process in the RGS will take place over a wide range of incident electron energies. Similar results have been observed in our laboratory for Kr and Xe substrates.[13] These results are clearly inconsistent with prediction (d). Finally, we may consider the possibility that the incident electron is inelastically scattered from the RGS to ~ 0 eV, and then becomes bound to the target molecule because of a positive electron affinity (as recently observed in Ar_nO_2 clusters[72]); it is conceivable that subsequent energy transfer from the newly created exciton could then excite the anion to the transient anion state which leads to DEA. However, an enhancement produced by this mechanism would be several eV broad,[72] and would have zero amplitude in the case of adsorbed C_2D_6, which has no low-lying anion states by which the very low-energy electron could be bound to the molecule.[39] This mechanism is therefore inconsistent with the experimental data.

From the above arguments, we may safely conclude that the observed structures in the anion desorption yields are inconsistent with any previously identified mechanisms for energy deposition in (and subsequent desorption from) the RGS. We therefore must reject the formation of excitons as participants in the enhanced desorption yields reported here. Our model for the formation of anion resonant states of the RGS is presented below, followed by the explanations of how the proposed anion states give rise to the experimental features and selectivity in the ESD yields.

VI. ANION STATES OF THE RARE-GAS ATOMS AND SOLIDS

The anionic resonances of isolated rare-gas atoms are well established; the $2\,^2S$ resonance state of He^{*-} at 19.367 ± 0.01 eV is now commonly used as a primary energy calibration in gas-phase electron-scattering experiments. In the case of the heavier rare gases, the lowest resonances are all $^2P_{3/2}$ states with the electronic configurations of $np^5(n+1)s^2$, where n is the highest occupied principal quantum number of the ground-state atom. The energies of these states are 11.098, 9.484, and 7.899 eV above the ground-state energy for Ar, Kr, and Xe, respectively.[15–17] The $^3P_0$ excited *neutral* states of these atoms, which represent the parent states of the resonances, are at 11.55, 9.92, and 8.32 eV, respectively.[73] The observation that the resonance states are *below* the energies of the parent states identifies the resonances as core-excited *Feshbach* states; the incident electron both excites the target atom and is trapped (bound) by the resulting electron–excited-state interaction potential. The only accessible decay channel for these lowest resonance states is by simultaneous emission of one $(n+1)s$ electron and relaxation of the remaining $(n+1)s$ electron to the normally occupied np atomic orbital; the formation of excited neutral states is not an energetically accessible channel. The limited number of decay channels implies both a relatively long lifetime for the resonance and a rather narrow energy spectrum for the formation of the resonance state (0.001–0.010 eV). Both characteristics are strongly contrasted with resonant states which are energetically above the parent state, i.e., core-excited *shape* resonances; these resonances can quickly decay by electron emission into the parent states, leading to broad excitation spectra.

The condensed phase equivalents of the neutral atomic excitations are commonly referred to as excitons. In principle, these states must be considered as excitations of the extended solid; however, the lowest-energy exci-

tons of the RGS can also be described in terms of mobile atomically based excitations[74,75] which can diffuse, or hop, through the solid.[10] The $n=1$ excitons in particular preserve much of their atomic nature; this interpretation is supported by the fact that the calculated effective orbital radii of the $(n+1)s$ electrons for the $n=1$ excitons in Ar, Kr, and Xe are only 0.48, 0.63, and 0.74 of the nearest-neighbor separations of the fcc lattice, respectively.[64] The diffusive motion can lead to long-range energy transport processes and it will continue until (a) the excitation is electronically relaxed (by photon emission), (b) the exciton becomes localized by self-trapping and phonon creation, or (c) the excitation is transferred to impurities in the solid. The most common fate of the exciton is self-trapping, which is followed by photon emission and relaxation to the ground state. Process (b) is known to occur with high probability in the RGS on the time scale of picoseconds, while process (c) will be extremely sensitive to the concentration of impurities in the solid. Zimmerer[65] has estimated that the excitons in condensed Ar, Kr, and Xe have mean diffusion radii of 50, 200, and 150 Å, respectively, prior to their eventual radiative decay. The tendency of the lighter RGS (Ne,Ar) to very rapidly self-trap leads to broad Gaussian absorption line shapes (FWHM $\sim$200 meV) and small diffusion radii, while the higher mobility of the Kr and Xe excitons is manifested in narrow Lorentzian absorption line shapes (FWHM $\sim$80 meV). The dynamics of exciton decay mechanisms in the RGS have recently been reviewed by Zimmerer.[65]

The lowest optically accessible excitons of the bulk RGS are the first of a Rydberg-type progression of exciton states which converge to the band gap of the solid. Consistent with the interpretation of the RGS exciton states as atomically based excitations, Resca *et al.*[74,75] have shown that all bulk exciton states of each RGS can be described as a Rydberg progression, with the dielectric constant of the solid modifying the electron-hole interaction potential. We will extend this atomic description of the excited states of the RGS by proposing the existence of anion resonance states in the RGS. To date, there have been no direct observations of such states, although Dalidchik and Slonim[18] have predicted that an anionic exciton band should exist in two-dimensional Xe layers; the calculated energy of this resonance was $\sim$0.5 eV *below* the neutral exciton band, suggesting that the incident electron would be bound to the excitation in much the same fashion as is found in the gas-phase resonances. The 0.5-eV binding energy of the electron to the neutral exciton is similar to the 0.4–0.5 eV for the gas-phase resonance states with respect to the lowest neutral excitation energies, and supports our use of models based on gas-phase atomic systems for the description of the excited states of the RGS.

By analogy with the resonances of the rare-gas atoms, we propose that the binding of the incident electron to the electronic excitation provides a mechanism for the simultaneous transport of energy *and charge* through the condensed phase. It is the interaction of these anionic excitons with adsorbed target species which give rise to the enhanced desorption yields. Excitations to the resonance states in the RGS would only be possible over a narrow range of energies corresponding to the discrete electron+excitation bound-state energy; at incident electron energies above the lowest exciton energies, the formation of long-lived resonance states would not be expected, since they are energetically capable of decaying into a free electron plus a neutral excitation. If the initial resonance state is formed in the bulk of the RGS (as opposed to at the surface), the probability of forming the anionic excitons would be determined by the thickness of the RGS. Further, we propose that the resonance state will diffuse, or hop, through the solid much like the neutral exciton, until (a) it decays by simultaneous electron emission and electronic relaxation to the ground state, (b) the resonance becomes self-trapped, or (c) it couples with impurities in or on the solid. It is known that the neutral excitations of the RGS will preferentially diffuse to (and decay at) the surface of the solid with approximately 4–8 higher probability than at subsurface layers.[76] The number of anionic excitons which reach the surface will therefore increase as the film thickness is increased until the thickness exceeds some characteristic diffusion length. Based on the results shown in Figs. 5 and 8, these lengths are of the order of 100–200 Å for Kr and Xe, and are comparable to the neutral exciton lengths for Kr and Xe.[65] The diffusion length for the anionic exciton in Ar is probably less than 20 Å, and again follows the trends previously reported for the neutral excitons; the larger width of the enhancement observed with Ar substrates probably reflects the increased trapping probability and has a direct parallel in the optical spectrum of solid Ar. The anticipated lifetime for a Feshbach-type resonance state is somewhat less than that of the neutral (nonlocalized) free exciton, and far less than the relaxation time of the trapped excitons ($\sim 10^{-9}$ s); it is therefore unlikely that the resonance state of the RGS will be relaxed prior to decay. If the resonance state did relax prior to the interaction with the adsorbed target species, the effective "electron energy" would be 1–2 eV less than that of the unrelaxed, mobile anionic exciton, based on the measured relaxation energies for the neutral excitons[65] as they self-trap. This would place the energy of the anionic exciton in solid Xe well below the 7.5-eV onset for DEA in adsorbed C_2D_6, *and therefore no enhancement would occur for this combination of target/RGS species.* The strong enhancements which *are* observed for this system demonstrate that *no relaxation takes place for those resonance excitations which lead to the enhanced ESD yields.* The present experiments are not sensitive to resonance states which become self-trapped and relaxed far from the target species (i.e., in the bulk).

The formation of mobile resonance states within the RGS, and their subsequent diffusion to the surface, can explain *a priori* the present observations by two somewhat different mechanisms. If the resonance states diffuse to the surface and then decay by autodetachment of the electron with its initial (unrelaxed) energy, the local free-electron current at the surface would be enhanced in direct proportion to the number of anionic excitations formed. The enhanced anion desorption yield via DEA would be increased only within the narrow en-

ergy band corresponding to the formation of the resonance state. Alternatively, it is also possible that the resonance state directly couples with the adsorbate species in order to lead to enhanced DEA probabilities and to an enhanced desorption yield; there is no free-electron intermediate in the second model. The first model cannot explain the lack of enhanced anion desorption yields from submonolayer O_2/Kr and O_2/Xe, the rapid decrease of the gain as the coverage of the rare-gas substrate by the target species is increased, nor the selectivity of the enhancement in the case of benzene overlayers. The sensitivity of the enhancement mechanism to the electronic structure of the adsorbate's dissociative states demands that there exists a direct coupling between the resonance state at the surface and the adsorbate. The mechanism of this coupling will be addressed below.

VII. MECHANISMS OF EXCITATION AND CHARGE TRANSFER

The following classes of the excitation+charge transfer (ECT) processes are involved in our experimental results:

$$X_a^{*-}+X_b \rightarrow X_a+X_b^{*-} , \tag{5a}$$

$$X^{*-}+AB \rightarrow X+AB^{*-} \text{ (dissociative)} , \tag{5b}$$

$$X^{*-}+AB \rightarrow X+AB^{*}+e^- , \tag{5c}$$

$$X+AB^{*-} \rightarrow X^{*}+AB+e^- , \tag{5d}$$

where X and AB represent an atomic and molecular species, respectively, $(X)^*$ denotes an electronically excited (X) species, and the subscripts distinguish identical species on different sites in the condensed phase. The probability for these ECT processes is proportional to the square of an interaction matrix element of the form $\langle \Phi_i | H_e | \Phi_f \rangle$, where H_e is the electronic Hamiltonian operator for the combined system of X_a+X_b or $X+AB$, and Φ_i and Φ_f are the initial- and final-state wave functions for the combined system. The electronic Hamiltonian H_e contains only one- and two-electron operators, and therefore the matrix element given above should vanish for three-electron processes, provided that the orbitals involved in the initial- Φ_i and final- Φ_f state wave functions are orthonormal to each other. All ECT processes (5a)–(5d) *formally* involve three-electron jumps and are therefore formally forbidden. We will show below that under special conditions some of the orbitals involved become nonorthogonal to each other and the *formal* three-electron jump becomes virtually a two-electron jump. Each of the ECT processes (5a)–(5d) is considered below along with a brief description of the related two-electron process. Note that the notation used to indicate the electronic configurations refers to *changes* in the orbital occupations with respect to the neutral, ground-state species [e.g., the $^2B_1$ state of H_2O is simply $(1b_1)^{-1}(3s{:}4a_1)^{+2}$].

A. Process (5a)

Process (5a) corresponds to the hopping of the (excitation plus charge) between identical atomic species in the condensed phase. In our experiments such a process is required if the initial site of the anion resonance in the RGS is not immediately adjacent to the adsorbed target molecules. The (excitation+charge) must have sufficient mobility to reach the surface, or to be mobile on the surface, in order to be transferred to the adsorbed molecules. In the case of Ar, Kr, or Xe solids, this ECT hopping process can be written as

$$X_a^{*-}[np_a^{-1}(n+1)s_a^{+2}]+X_b \rightarrow X_a+X_b^{*-}[np_b^{-1}(n+1)s_b^{+2}] , \tag{6}$$

where $n=3,4,5$ for Ar, Kr, and Xe, respectively. The hopping probability of the ECT process (6) is approximately equal to $|\langle (n+1)s_a|(n+1)s_b\rangle|^2 T_2$, where T_2 is a hopping probability for a corresponding two-electron exciton transport process:

$$X_a^{*}[np_a^{-1}(n+1)s_a^{+1}]+X_b \rightarrow X_a+X_b^{*}[np_b^{-1}(n+1)s_b^{+1}] . \tag{7}$$

The overlap integral $\langle (n+1)s_a|(n+1)s_b\rangle$ does not vanish because $(n+1)s_a$ and $(n+1)s_b$ are both Rydberg-type orbitals. It is shown in the Appendix that Rydberg-type orbitals belonging to adjacent atoms are not necessarily orthogonal to each other. The $\langle (n+1)s_a|(n+1)s_b\rangle$ overlap integral is probably the main cause for the relative hopping efficiency for the three rare-gas solids studied in this experiment (Ar $\ll$ Kr $<$ Xe). The spatial overlap of the exciton radii with the nearest-neighbor atoms of the solid follow precisely the same sequence as mentioned above.

In the case of a *valence* anionic excitation, e.g., the $^2\Pi_u$ state of $O_2^{-}(1\pi_u)^{-1}(1\pi_g)^{+2}$ in condensed O_2, the three-electron hopping probability will be negligibly small since the overlap of the valence orbitals for adjacent O_2 molecules is negligibly small. Thus *valence* one-hole two-particle resonances do not hop in the solid.

B. Process (5b)

ECT between dissimilar species (e.g., Kr and H_2O) can occur when the discrete energies of the initial and final states of the system are precisely equal. In the case of a transfer from an atomic excitation (with a narrow energy spectrum) to a molecular target species, this equivalence is much more probable if the anionic state of the molecular species is dissociative and thereby has a broad energy spectrum for a Franck-Condon transition from the ground-state molecule. These dissociative, excited anion states of the target molecules have been extensively explored via dissociative electron attachment studies for many species in the gas phase,[77] and more recently, in the condensed phase.[78]

The transfer of an atomic Rydberg anion excitation to a dissociative molecular Rydberg state, i.e.,

$$X^{*-}[np^{-1}(n+1)s^{+2}]+AB \rightarrow X+AB^{*-}[V^{-1}R^{+2}] , \tag{8}$$

can have a nonzero transition probability, as shown in

the Appendix. Orbital R denotes a low-lying Rydberg orbital, while V denotes one of the normally occupied valence orbitals. As before, the probability for ECT process (8) is approximately given by $T_3 = |\langle (n+1)s|R\rangle|^{2*} T_2$, where T_2 is a transfer probability for the corresponding two-electron process,

$$X^*[np^{-1}(n+1)s^{+1}] + AB \rightarrow X + AB^*[V^{-1}R^{+1}] . \quad (9)$$

Notice that $AB^*[V^{-1}R^{+1}]$ represents a neutral dissociative Rydberg state, such as the $^1B_1$ state of H_2O.

In the case of a transition from an atomic Rydberg anion excitation to a dissociative molecular valence state, e.g.,

$$Kr^{*-}[4p^{-1}5s^{+2}] + O_2 \rightarrow Kr + O_2^{*-}[1\pi_u^{-1}1\pi_g^{+2}] , \quad (10)$$

the transition probability remains negligibly small because of the near orthogonality of the Rydberg orbital $5s'$ with the valence orbitals of O_2. This point is explained in the Appendix. The absence of enhanced anion yields found for DEA involving valence states of the target molecule arises from the negligibly small ECT probability described above.

C. Process (5c)

Process (5c) is clearly analogous to that of process (5b), with the key difference being that one of the electrons in the final state is in a quasifree continuum, propagating through the medium. As a result, the transfer probability for the ECT process

$$X^{*-}[np^{-1}(n+1)s^{+2}] + AB \rightarrow X + AB^*[V^{-1}R^{+1}] + e^- \quad (11)$$

is approximately given by $T_3 = |\langle (n+1)s|R\rangle|^{2*} T_2$, where T_2 is the transfer probability for the two-electron process

$$X^*[np^{-1}(n+1)s^{+1}] + AB \rightarrow AB^+[V^{-1}] + e^- . \quad (12)$$

We emphasize that R represents a Rydberg orbital and hence $AB^*[V^{-1}R^{+1}]$ represents a Rydberg state. Process (11) will compete with process (8) when both are energetically allowed.

D. Process (5d)

This process is essentially the same phenomenon as process (5c), where the roles of the atomic and molecular states interchanged. We include this process to show the close relationship between processes (5d) and (5b). The electron detachment process from a molecular Rydberg anionic state

$$X + AB^{*-}[V^{-1}R^{+2}] \rightarrow X^*[np^{-1}(n+1)s^{+1}] + AB + e^- \quad (13)$$

is thereby allowed, with a three-electron transfer probability given by $T_3 = |\langle (n+1)s|R\rangle|^{2*} T_2$, where T_2 is the transition probability of the related two-electron process

$$X + AB^*[V^{-1}R^{+1}] \rightarrow X^+[np^{-1}] + AB + e^- . \quad (14)$$

Process (13) is almost a reversal of process (8). The ratio of the transfer rates for processes (13) and (8) is approximately equal to that for the corresponding two-electron processes, namely

$$T_3\ (13)/T_3\ (8) \sim T_2\ (14)/T_2\ (9) \quad (15)$$

because the associated overlap integrals are the same.

Since two-electron transfer rates T_2 (14) and T_2 (9) are expected to be of comparable magnitude, we expect that rates for T_3 (13) and T_3 (8) will also be similar. In other words, when the process (8) is observed, the corresponding reverse process (13) is also expected to occur. When the $AB^{*-}[V^{-1}R^{+2}]$ of process (13) is dissociative, process (13) represents a quenching of DEA via the $AB^{*-}[V^{-1}R^{+2}]$ resonance state. Since process (13) is active only above the $X^*[np^{-1}(n+1)s^{+1}]$ exciton formation energy, this quenching of DEA should be seen immediately above the enhancement energy feature which arises from the $X^{*-}(np^{-1})(n+1)s^{+2}$ resonance.

E. Two-electron transfer processes

The above-mentioned two-electron transfer processes (7), (9), and (12) are well-established processes. Process (7) is simply the hopping of excitations in the RGS, which has been seen clearly in several experiments,[10,65] usually by the anomalously large luminescence (or photoelectron) yields from dilute dopants in the RGS. Process (9) is a dissociative excitation transfer which has been reported for molecular species in rare-gas matrices. Process (12) is simply Penning ionization, which is a mechanism leading to charge separation in the RGS.[7,8] The remaining two-electron process, shown as (14), is rare, simply because it is more difficult to prepare a long-lived AB^* in a well-defined energy than to prepare a long-lived excitation of the rare-gas host.

VIII. CONCLUSION

The results and theoretical model presented here demonstrate that it is possible to create anionic excitons by electron impact in the rare-gas solids; the formation of these core-excited resonance states is modeled on the established mechanism for the formation of anionic excitations (resonances) of the rare-gas atoms, and the motion of these anionic excitations in the condensed phase is modeled on the established dynamics of neutral excitons in the rare-gas solids. These states can couple selectively with dissociative Rydberg states of adsorbed molecules, yet do not couple with dissociative valence states. This characteristic may allow the use of these resonances to experimentally determine the magnitude of the Rydberg contributions for dissociative states of more complex molecules; it is often difficult to make such determinations based exclusively on optical data.[36] To the best of our knowledge, the enhancements of the anion desorption yields which are caused by this mechanism are the narrowest features yet observed for ESD.

Anionic excitations of the rate-gas solids provide a mechanism for the quasielastic transport of energy and charge through the condensed phase. As mentioned in

the Introduction, exciton relaxation processes can often complicate the interpretation of energy transport results using neutral excitons;[65] it is possible that the study of anionic excitations of the RGS can circumvent these difficulties, and therefore enhance the study of energy and charge transport phenomena in the condensed phase.

ACKNOWLEDGMENTS

Funding for this research has been provided by the Canadian Medical Research Council, the Canadian Centre of Excellence in Molecular and Interfacial Dynamics, and by the Office of Naval Research. One of us (P.R.) gratefully acknowledges the support of the Canadian Natural Sciences and Engineering Research Council.

APPENDIX

Let us first consider one conceivable example of process (5b) whereby an anionic excitation of solid Xe interacts with ground state O_2, leading to the formation of the dissociative $^2\Pi_u O_2^-$ anion, i.e.,

$$Xe^{*-}[5p^{-1}6s^{+2}]+O_2 \rightarrow Xe+O_2^{*-}[1\pi_u^{-1}1\pi_g^{+2}] . \quad (A1)$$

Here we will assume that the separation between the Xe and the O_2 is the sum of their van der Waals radii. This implies that the *valence* orbitals of Xe (i.e., $5p$ and lower) have negligible overlap with the valence orbitals of O_2 (i.e., $1\pi_g$ and lower). It is expected that the shape of the valence orbitals, unlike the orbital energies, are almost independent of the electronic configuration used to obtain the valence orbitals, implying that the $1\pi_g$ and lower lying orbitals obtained for the O_2^{*-} have almost the same shape as those obtained for O_2, and that the $5p$ and lower-lying orbitals of Xe^{*-} are essentially identical to those of Xe. [This expectation arises from the following considerations: (i) The major change in the valence orbitals occurs because of the changes in the electrostatic potential within the region occupied by the valence orbitals. (ii) Electrons occupying the Rydberg orbitals produce a nearly constant potential within the valence region. (iii) The electrostatic potential is determined by the integration of the electronic charge distribution across the space of the orbital(s), so that it is relatively insensitive to the details of the charge distribution. The result of these considerations is that the alteration in the valence orbitals induced by changes in the electronic configuration is largely restricted to the *energetics* of the orbitals, and does not include dramatic changes to the *shapes* of the orbitals.] In short the valence orbitals of isolated Xe and isolated O_2 are very good solutions for both $[Xe^{*-}:O_2]$ and $[Xe:O_2^{*-}]$ complexes and therefore the valence orbitals of $[Xe^{*-}:O_2]$ are almost identical to those of $[Xe:O_2^{*-}]$.

In contrast, the $6s$ Rydberg orbital of isolated Xe^{*-} is *not* a good solution for an orbital of the $[Xe^{*-}:O_2]$ complex because of a large spatial overlap between the $6s$ Rydberg orbital and the valence orbitals of O_2. Nonetheless, there is an orbital of $[Xe^{*-}:O_2]$, which we will denote $6s'$, that is clearly derived from the $6s$ orbital of the atomic Xe^{*-}. This $6s'$ orbital is orthogonal to all other (Rydberg and valence) orbital solutions for $[Xe^{*-}:O_2]$, but is not necessarily orthogonal to the orbital solutions for $[Xe:O_2^{*-}]$. The $6s'$ orbital remains almost orthogonal to the valence orbitals of $[Xe:O_2^{*-}]$ because the valence orbitals of $[Xe^{*-}:O_2]$ are almost identical to the valence orbitals of $[Xe:O_2^{*-}]$, as discussed above. All of the occupied orbitals in $[Xe:O_2^{*-}]$ are valencelike. Furthermore, orbitals occupied in $[Xe:O_2^{*-}]$ are also occupied in $[Xe^{*-}:O_2]$. Consequently, all of the occupied orbitals in $[Xe^{*-}:O_2]$ and $[Xe:O_2^{*-}]$ are almost orthogonal to each other. This near orthogonality makes the three-electron jump probability for process (A1) negligibly small. It is for this reason that O^- desorption from submonolayer O_2/Kr and O_2/Xe does not show a resonance enhancement in the anion yields.

Let us consider another case of process (5b), that is,

$$Xe^{*-}[5p^{-1}6s^{+2}]+CO \rightarrow Xe+CO^{*-}[V^{-1}2\pi^{+2}] . \quad (A2)$$

In the case of (A1), valence orbitals occupied in $[Xe:O_2^{*-}]$ are also occupied in $[Xe^{*-}:O_2]$ without exception. In the present case (A2), however, the 2π valence orbital which is occupied in $[Xe:CO^{*-}]$ is not occupied in $[Xe^{*-}:CO]$. Following the arguments given for (A1), we may still conclude that the $6s'$ orbital of $[Xe^{*-}:CO]$ is almost orthogonal to all valence orbitals occupied in $[Xe:CO^{*-}]$ except the 2π valence orbital. Our task is to estimate the overlap integral between the $6s'$ and the 2π orbitals. An operator for orbitals (such as the Fock operator in the Hartree-Fock formalism or the effective one-electron operator in the $X\alpha$ method) yields not only occupied orbitals but also unoccupied orbitals, so-called virtual orbitals. Among the virtual orbitals, occasionally there exist orbitals that are localized similarly to other valence orbitals and have relatively low orbital energies. We shall refer to this as a "virtual valence orbital." The operator for $[Xe^{*-}:CO]$ yields such a virtual valence orbital $2\pi'$, which is almost the same as the 2π valence operator of $[Xe:CO^{*-}]$. Since $6s'$ and $2\pi'$ are solutions of a single operator, they are orthogonal to each other. Consequently, we can conclude that the ns' and 2π orbitals are almost orthogonal to each other. Thus process (A2), as well as (A1), is forbidden to a first approximation.

Let us now turn to the third case of process (5b),

$$X^{*-}[np^{-1}(n+1)s'^{+2}]+AB \rightarrow X+AB^{*-}[V^{-1}R'^{+2}] . \quad (A3)$$

The critical difference between (A3) and (A2) is that the orbital R in (A3) is a Rydberg orbital, while the 2π orbital is a valence orbital. Following the argument given for process (A1), we may conclude that (i) the $(n+1)s'$ orbital of $[X^{*-}:AB]$ is almost orthogonal to all valence orbitals occupied in $[X:AB^{*-}]$; (ii) the R' orbital of $[X:AB^{*-}]$ is almost orthogonal to all valence orbitals occupied in $[X^{*-}:AB]$; and (iii) the valence orbitals occupied in $[X:AB^{*-}]$ are almost identical to those of $[X^{*-}:AB]$. Thus the unknown overlap integral is $\langle (n+1)s'|R'\rangle$. If the R' orbital of $[X:AB^{*-}]$ is almost the same as the one of the virtual orbitals of $[X^{*-}:AB]$,

or if the ns' orbital of $[X^{*-}:AB]$ is almost the same as the virtual orbitals of $[X:AB^{*-}]$, then the integral $\langle ns'|R'\rangle$ would be negligibly small. This is not the case, however, because the R orbital of AB^{*-} differs significantly from all virtual orbitals of AB (and also because the ns orbital of X^{*-} differs from any virtual orbitals of X). The electron(s) in the Rydberg orbital R is largely outside of the molecular region and move under the Coulomb influence of the $AB^{+}[V^{-1}]$ core. AB (and also $AB^{*}[V_1^{-1}V_2]$, where V_1,V_2 are valence orbitals) cannot support Rydberg orbitals, since there is no net positive core by which they could be bound. Similarly, we can argue that X cannot accommodate Rydberg orbitals. In short, there is no reason for the $\langle (n+1)s'|R'\rangle$ of (A3) to be negligibly small, in contrast to the $\langle 6s'|2\pi\rangle$ of (A2).

The allowed cases of (5a), (5c), and (5d), that is, processes (6), (11), and (13), are all due to a nonvanishing overlap integral between Rydberg orbitals belonging to different atoms or molecules. This nonorthogonality of Rydberg orbitals for the above cases can be shown by following the same line of argument as presented for (A3).

[1]Z. Lu, M. T. Schmidt, D. V. Podlesnik, C. F. Yu, and R. M. Osgood, Jr., J. Chem. Phys. **93**, 7951 (1990).
[2]F. Bozso and Ph. Avouris, Phys. Rev. B **44**, 9129 (1991).
[3]Y. Chen, J. M. Seo, F. Stepniak, and J. H. Weaver, J. Chem. Phys. **95**, 8442 (1991).
[4]St. J. Dixon-Warren, J. C. Polanyi, C. D. Stanners, and G.-Q. Xu, J. Phys. Chem. **94**, 5664 (1990).
[5]E. P. Marsh, T. L. Gilton, W. Meier, M. R. Schneider, and J. P. Cowin, Phys. Rev. Lett. **61**, 2725 (1988).
[6]S. K. Jo and J. M. White, J. Phys. Chem. **94**, 6852 (1990).
[7]M. E. Fajardo and V. A. Apkarian, J. Chem. Phys. **85**, 5660 (1986).
[8]M. E. Fajardo and V. A. Apkarian, J. Chem. Phys. **89**, 4102 (1988).
[9]N. Schwentner and E. E. Koch, Phys. Rev. B **14**, 4687 (1976).
[10]Z. Ophir, B. Raz, J. Jortner, V. Saile, N. Schwentner, E.-E. Koch, M. Skibowski, and W. Steinmann, J. Chem. Phys. **62**, 650 (1975).
[11]E. E. Koch and M. Skibowski, Chem. Phys. Lett. **9**, 429 (1971).
[12]R. Kopelman, E. M. Monberg, F. W. Ochs, and P. N. Prasad, Phys. Rev. Lett. **34**, 1506 (1975).
[13]G. Leclerc, A. D. Bass, M. Michaud, and L. Sanche, J. Electron Spectrosc. Relat. Phenom. **52**, 725 (1990).
[14]L. Sanche, J. Phys. B **23**, 1597 (1990).
[15]L. Sanche and G. J. Schulz, Phys. Rev. A **5**, 1672 (1972).
[16]A. Weingartshofer, K. Willman, and E. M. Clarke, J. Phys. B **7**, 79 (1974).
[17]J. N. H. Brunt, G. C. King, and F. H. Read, J. Phys. B **10**, 1289 (1977).
[18]F. I. Dalidchik and V. Z. Slonim, Pis'ma Zh. Eksp. Teor. Fiz. **31**, 122 (1980) [JETP Lett. **31**, 112 (1980)].
[19]R. W. Munn, W. G. Mabbott, and M. Pope, Chem. Phys. **139**, 339 (1989).
[20]D. S. Bélic, M. Landau, and R. I. Hall, J. Phys. B **14**, 175 (1981).
[21]V. Engel, R. Schinke, and V. Staemmler, J. Chem. Phys. **88**, 129 (1988).
[22]C. E. Melton, J. Chem. Phys. **57**, 4218 (1972).
[23]R. N. Compton and L. G. Christophorou, Phys. Rev. **154**, 110 (1967).
[24]R. Azria, L. Parenteau, and L. Sanche, J. Chem. Phys. **87**, 2292 (1987).
[25]L. Sanche, L. Parenteau, and P. Cloutier, J. Chem. Phys **91**, 2664 (1989).
[26]P. Rowntree, L. Parenteau, and L. Sanche, J. Chem. Phys. **94**, 8570 (1991).
[27]P. Rowntree, L. Parenteau, and L. Sanche, J. Phys. Chem. **95**, 4902 (1991).
[28]D. Roy and D. Tremblay, Rep. Prog. Phys. **53**, 1621 (1990).
[29]P. Cloutier (private communication).
[30]M. Michaud and L. Sanche, Phys. Rev. A **36**, 4684 (1987).
[31]T. Shibaguchi, H. Onuki, and R. Onaka, J. Phys. Soc. Jpn. **42**, 152 (1977).
[32]M. Bernheim and T. Wu (unpublished).
[33]M. Tronc, S. Goursaud, R. Azria, and F. Fiquet-Fayard, J. Phys. **34**, 381 (1973).
[34]F. H. Dorman, J. Chem. Phys. **44**, 3856 (1966).
[35]J. W. Raymonda and W. T. Simpson, J. Chem. Phys. **47**, 430 (1967).
[36]M. B. Robin, *Higher Excited States of Polyatomic Molecules* (Academic, New York, 1975 and 1985), Vols. I, II, and III.
[37]R. J. Buenker and S. D. Peyerimhoff, Chem. Phys. **8**, 56 (1975).
[38]C. Sandorfy, Z. Phys. Chem. Neue Folge **101**, 307 (1976).
[39]K. D. Jordan and P. Burrow, Chem. Rev. **87**, 557 (1987).
[40]H.-P. Fenzlaff and E. Illenberger, Int. J. Mass Spectrosc. Ion Proc. **59**, 185 (1984).
[41]L. von Trepka and H. Neuert, Z. Naturforsch. A **18**, 1295 (1963).
[42]P. G. Wilkinson, Can. J. Phys. **34**, 596 (1956).
[43]M. Allan, Helv. Chim. Acta **65**, 2008 (1982).
[44]L. Sanche and M. Michaud, Chem. Phys. Lett. **80**, 184 (1981).
[45]B. Katz, M. Brith, B. Sharf, and J. Jortner, J. Chem. Phys. **50**, 5195 (1969).
[46]J. G. Angus and G. C. Morris, Mol. Cryst. Liq. Cryst. **11**, 309 (1970).
[47]R. Azria and G. J. Schulz, J. Chem. Phys. **62**, 573 (1975).
[48]M. Allan, J. Electron. Spectrosc. Relat. Phenom. **48**, 219 (1989).
[49]D. Rapp and D. D. Briglia, J. Chem. Phys. **43**, 1480 (1965).
[50]R. Azria, L. Parenteau, and L. Sanche, Phys. Rev. Lett. **59**, 638 (1987).
[51]H. Sambe and D. E. Ramaker, Phys. Rev. A **40**, 3651 (1989).
[52]R. Hashemi and E. Illenberger, Chem. Phys. Lett. **187**, 623 (1991).
[53]E. M. Hörl, J. Mol. Spectrosc. **3**, 548 (1959).
[54]A. M. Bass and H. P. Broida, J. Mol. Spectrosc. **12**, 221 (1964).
[55]P. Rowntree, L. Parenteau, and L. Sanche, Chem. Phys. Lett. **182**, 479 (1991).
[56]M. Michaud, P. Cloutier, and L. Sanche, Phys. Rev. A **44**, 5624 (1991).
[57]M. Knapp, O. Echt, D. Kreisle, and E. Recknagel, J. Phys. Chem. **91**, 2601 (1987).
[58]M. Knapp, O. Echt, D. Kreisle, and E. Recknagel J. Chem. Phys. **85**, 636 (1986).
[59]W. H. Press, B. P. Flannery, S. A. Teukolsky, and W. T.

Vetterling, *Numerical Recipes in Pascal* (Cambridge University Press, Cambridge, 1989).
[60]L. Sanche, Comments At. Mol. Phys. **26**, 321 (1991).
[61]M. Michaud and L. Sanche, J. Electron. Spectrosc. Relat. Phenom. **51**, 237 (1990).
[62]H. Sambe, D. E. Ramaker, L. Parenteau, and L. Sanche, Phys. Rev. Lett. **59**, 236 (1987).
[63]F. Coletti, J. M. Debever, and G. Zimmerer, J. Phys. Lett. **45**, L467 (1984).
[64]N. Schwentner, E.-E. Koch, and J. Jortner, *Electronic Excitations in Condensed Rare Gases* (Springer-Verlag, Berlin, 1985).
[65]G. Zimmerer, *Excited State Spectroscopy in Solids,* edited by U. M. Grassono and N. Terzi (North-Holland, Amsterdam, 1987).
[66]L. Sanche and M. Deschenes, Phys. Rev. Lett. **61**, 2096 (1988).
[67]A. D. Bass and L. Sanche, J. Chem. Phys. **95**, 2910 (1991).
[68]H. Sambe, D. E. Ramaker, M. Deschenes, A. D. Bass, and L. Sanche, Phys. Rev. Lett. **64**, 523 (1990).
[69]M. Pope, H. Kallman, and J. Giachimo, J. Chem. Phys. **42**, 2540 (1965).
[70]M. Pope and J. Burgos, J. Mol. Cryst. **1**, 295 (1966).
[71]G. T. Pott and D. F. Williams, J. Chem. Phys. **51**, 203 (1969).
[72]M. Foltin, G. Walder, A.W. Castleman, Jr., and T. D. Märk, J. Chem. Phys. **94**, 810 (1991).
[73]C. E. Moore, *Atomic Energy Levels,* Natl. Bur. Stand. (U.S.) Circ. No. 467 (U.S. GPO, Washington, DC, 1949), Vol. 1.
[74]L. Resca, R. Resta, and S. Rodriguez, Phys. Rev. B **18**, 696 (1978).
[75]L. Resca and R. Resta, Phys. Rev. B **19**, 1683 (1979).
[76]J. W. Boring, R. E. Johnson, and D. J. O'Shaughnessy, Phys. Rev. B **39**, 2689 (1989).
[77]L. G. Christophorou, *Atomic and Molecular Radiation Physics* (Wiley, Brussels, 1971).
[78]L. Sanche, in *Excess Electrons in Dielectric Media,* edited by C. Ferradini and J.-P. Jay-Gerin (CRC, Boca Raton, FL, 1990), Chap. 1.